A dynamic global-coefficient subgrid-scale eddy-viscosity model for large-eddy simulation in complex geometries

By D. You AND P. Moin

1. Motivation and objectives

A major drawback of the Smagorinsky subgrid-scale eddy-viscosity model used in large-eddy simulations is that the model needs to be closed with an empirical constant, which has been found far from being universal and difficult to adjust to the characteristics of the turbulent flow field and computational resolution (Germano *et al.* 1991). Furthermore, the Smagorinsky model predicts non-vanishing subgrid-scale eddy viscosity in the regions where the flow is laminar, or the eddy viscosity should be zero. These shortcomings of the Smagorinsky model were overcome by Germano *et al.* (1991) through a dynamic procedure for determining the model coefficient. In the dynamic Smagorinsky model, the model coefficient is dynamically determined as a function of space and time using the scale-invariance concept and the "local-equilibrium" hypothesis (i.e., an equilibrium between the subgrid-scale dissipation and the viscous dissipation at the same physical location).

Although the dynamic model coefficient vanishes where the flow is laminar or fully resolved, it can cause numerical instability since its value often becomes negative and/or highly fluctuates in space and time. The numerical instability is remedied by additional numerical procedures such as an averaging of the model coefficient over statistically homogeneous directions or an ad hoc clipping procedure. The numerical stabilization procedure becomes complicated when the dynamic model is applied to a complex flow configuration in which there are no homogeneous directions. A number of novel approaches have been proposed (e.g., the dynamic localization model by Ghosal *et al.* (1994) and the Lagrangian dynamic model by Meneveau *et al.* (1996)) to address this issue. For example, the Lagrangian dynamic subgrid-scale model has been successfully employed for large-eddy simulations of flow through a real jet engine combustor (Moin 2002) and the tip-leakage flow in a turbomachinery cascade (You *et al.* 2004). However, the iterative solution procedure to solve an integral equation in the dynamic localization procedure (Ghosal *et al.* 1994) or the interpolation required for the pathline averaging in the Lagrangian dynamic model (Meneveau *et al.* 1996) demands a non-trivial effort in implementation, results in computational overhead, and may still require non-physical clipping operations.

Recently, Vreman (2004) developed a new subgrid-scale eddy-viscosity model that appears to offer several advantages over the Smagorinsky model with a constant coefficient. In this model, vanishing subgrid-scale dissipation for various laminar shear flows is theoretically guaranteed even with a non-zero constant empirical model coefficient. Since the model provides desirable features for successful large-eddy simulation even with a spatially uniform model coefficient and does not require any averaging or clipping procedures for numerical stabilization, it is especially suitable for complex flow configurations. Vre-

man (2004) showed that the model with a fixed coefficient predicts turbulence statistics for channel flow without introducing any wall-damping functions.

However, more recently, Park *et al.* (2006) showed that the model coefficient is not universal for all turbulent flows and needs to be adjusted according to the turbulent flow field simulated. They proposed a dynamic procedure for determining the model coefficient utilizing the "global equilibrium" between the subgrid-scale dissipation and the viscous dissipation (da Silva & Metais 2002). In this approach, the model coefficient is globally constant in space but varies in time, and it still guarantees zero eddy viscosity in the laminar-flow regions. Furthermore, the model does not require any ad hoc numerical stabilization or clipping operations. The dynamic procedure was found quite effective in determining the model coefficient and predicted superior results to those obtained by using the fixed-coefficient Smagorinsky model in a number of applications including turbulent channel flow and flows over a circular cylinder and a sphere (Park *et al.* 2006).

In this study, we propose an improvement of the dynamic global-coefficient subgrid-scale eddy-viscosity model of Park *et al.* (2006). The present dynamic procedure is also based on the "global equilibrium" between the subgrid-scale and viscous dissipation. In contrast to the dynamic procedure of Park *et al.* (2006) which requires two-level test filters, the present model requires only a single-level test filter, and therefore is more suitable for large-eddy simulation in complex geometries. The present dynamic procedure guarantees a model coefficient which is free from the influence of the computational domain size over which the volume averaging is taken while it is controlled by a scale-invariance concept in the model of Park *et al.* (2006).

The original Vreman model and the dynamic model of Park *et al.* (2006) are briefly introduced in section 2. Then, in section 3, the present dynamic model is derived and its characteristics are discussed. In section 4, the predictive capability of the present model is evaluated by considering turbulent channel flow and flow over a circular cylinder. A brief summary is presented in section 5.

2. Vreman-type subgrid-scale eddy-viscosity models

The incompressible Navier-Stokes and continuity equations are:

$$\frac{\partial u_i}{\partial t} = -\frac{\partial u_i u_j}{\partial x_j} - \frac{\partial p}{\partial x_i} + \nu \frac{\partial^2 u_i}{\partial x_j \partial x_j}, \tag{2.1}$$

$$\frac{\partial u_i}{\partial x_i} = 0. \tag{2.2}$$

By applying a "grid" filter $\overline{()}$ to (2.1) and (2.2), one obtains the filtered equations of motions

$$\frac{\partial \overline{u}_i}{\partial t} = -\frac{\partial \overline{u}_i \overline{u}_j}{\partial x_j} - \frac{\partial \overline{p}}{\partial x_i} + \nu \frac{\partial^2 \overline{u}_i}{\partial x_j \partial x_j} - \frac{\partial \tau_{ij}}{\partial x_j}, \tag{2.3}$$

$$\frac{\partial \overline{u}_i}{\partial x_i} = 0, \tag{2.4}$$

where τ_{ij} is the subgrid-scale stress tensor. The subgrid-scale stress tensor τ_{ij} is modeled by an eddy-viscosity model:

$$\tau_{ij} - \frac{1}{3}\delta_{ij}\tau_{ij} = -2\nu_T \overline{S}_{ij}, \tag{2.5}$$

where ν_T is the eddy viscosity. In the present study, the Vreman-type eddy-viscosity models are considered for determining ν_T.

2.1. *Subgrid-scale model with a fixed model coefficient*

Vreman (2004) proposed a subgrid-scale eddy-viscosity model for ν_T in the following form:

$$\nu_T = C_v \bar{\Pi}, \tag{2.6}$$

where

$$\bar{\Pi} = \sqrt{\frac{\overline{B}_\beta}{\overline{\alpha}_{kl}\overline{\alpha}_{kl}}},$$

$$\overline{B}_\beta = \overline{\beta}_{11}\overline{\beta}_{22} - \overline{\beta}_{12}\overline{\beta}_{12} + \overline{\beta}_{11}\overline{\beta}_{33} - \overline{\beta}_{13}\overline{\beta}_{13} + \overline{\beta}_{22}\overline{\beta}_{33} - \overline{\beta}_{23}\overline{\beta}_{23},$$

$$\overline{\beta}_{ij} = \sum_{m=1}^{3} \overline{\Delta}_m^2 \overline{\alpha}_{mi}\overline{\alpha}_{mj},$$

$$\overline{\alpha}_{ij} = \frac{\partial \overline{u}_j}{\partial x_i}, \tag{2.7}$$

$\overline{\Delta}_m$ is the grid-filter width in the m-direction, and C_v is the model coefficient. A novel feature of the model that makes it superior to the Smagorinsky model with a constant coefficient, is that the kernel $\bar{\Pi}$ becomes zero for canonical cases where the eddy viscosity should be zero. More details of the derivation of the model and its characteristics can be found in Vreman (2004).

For homogeneous turbulent flow, Vreman (2004) proposed C_v of 0.07 and showed favorable results. However, the value is found not universal and needs to be adjusted according to the flow and computational resolution as noted by Park *et al.* (2006).

2.2. *Dynamic model with two-level test filters*

Park *et al.* (2006) proposed a dynamic procedure for the determination of the model coefficient. They considered a transport equation for τ_{ii} $(= \overline{u_i u_i} - \overline{u}_i\overline{u}_i)$:

$$\frac{\partial \tau_{ii}}{\partial t} = \underbrace{\frac{\partial}{\partial x_j}\left\{-(\overline{u_i u_i u_j} - \overline{u}_i\overline{u}_i\overline{u}_j) - 2(\overline{u_j p} - \overline{u}_j\overline{p}) + \nu\left(\frac{\partial \overline{u_i u_i}}{\partial x_j} - \frac{\partial \overline{u}_i\overline{u}_i}{\partial x_j}\right) + 2\tau_{ij}\overline{u}_i\right\}}_{\Gamma}$$
$$\underbrace{-2\nu\left(\overline{\frac{\partial u_i}{\partial x_j}\frac{\partial u_i}{\partial x_j}} - \frac{\partial \overline{u}_i}{\partial x_j}\frac{\partial \overline{u}_i}{\partial x_j}\right)}_{\varepsilon_\nu} - \underbrace{2\tau_{ij}\overline{S}_{ij}}_{\varepsilon_{SGS}}, \tag{2.8}$$

where Γ is the redistribution term, and ε_ν and ε_{SGS} are the viscous and the subgrid-scale dissipation terms, respectively. Taking the volume average $\langle\rangle$ of the terms in (2.8) over the entire computational domain yields

$$\left\langle \tau_{ij}\overline{S}_{ij} \right\rangle = -\nu \left\langle \overline{\alpha_{ij}\alpha_{ij}} - \overline{\alpha}_{ij}\overline{\alpha}_{ij} \right\rangle, \tag{2.9}$$

assuming the volume averages of the redistribution term and the time variation of τ_{ii} are negligible (Piomelli *et al.* 1996; da Silva & Metais 2002; Park *et al.* 2006). The relationship in (2.9) was referred to as the "global equilibrium" between the viscous dissipation and the subgrid-scale dissipation (Park *et al.* 2006; da Silva & Metais 2002). da Silva & Metais (2002) and Park *et al.* (2006) found that the equilibrium between the viscous and subgrid-scale dissipation is only observed "globally" (not locally).

Replacing τ_{ij} in (2.9) with (2.6) results in

$$C_v = \frac{\nu}{2} \cdot \frac{(\gamma - 1)\,\langle \overline{\alpha}_{ij}\overline{\alpha}_{ij} \rangle}{\langle \bar{\Pi}\bar{S}_{ij}\bar{S}_{ij} \rangle}, \tag{2.10}$$

where the following closure assumption has been made

$$\langle \overline{\alpha_{ij}\alpha_{ij}} \rangle = \gamma \,\langle \overline{\alpha}_{ij}\overline{\alpha}_{ij} \rangle \,. \tag{2.11}$$

The model uses the following scale-invariance assumption:

$$\gamma = \frac{\langle \overline{\alpha_{ij}\alpha_{ij}} \rangle}{\langle \overline{\alpha}_{ij}\overline{\alpha}_{ij} \rangle} = \kappa \frac{\langle \overline{\alpha}_{ij}\overline{\alpha}_{ij} \rangle}{\langle \widetilde{\alpha}_{ij}\widetilde{\alpha}_{ij} \rangle} \approx \kappa^2 \frac{\langle \widetilde{\alpha}_{ij}\widetilde{\alpha}_{ij} \rangle}{\langle \widehat{\alpha}_{ij}\widehat{\alpha}_{ij} \rangle}, \tag{2.12}$$

where κ is another unknown parameter to be determined together with γ. $\widetilde{\alpha}_{ij}$ and $\widehat{\alpha}_{ij}$ are the first- and second-level test-filtered tensors, respectively, and $\widetilde{\Delta} = 2\overline{\Delta}$ and $\widehat{\Delta} = 2\widetilde{\Delta}$ are assumed. From (2.12), κ and γ are readily obtained as follows:

$$\kappa = \frac{\langle \widehat{\alpha}_{ij}\widehat{\alpha}_{ij} \rangle \,\langle \overline{\alpha}_{ij}\overline{\alpha}_{ij} \rangle}{\langle \widetilde{\alpha}_{ij}\widetilde{\alpha}_{ij} \rangle^2}, \qquad \gamma = \frac{\langle \widehat{\alpha}_{ij}\widehat{\alpha}_{ij} \rangle \,\langle \overline{\alpha}_{ij}\overline{\alpha}_{ij} \rangle^2}{\langle \widetilde{\alpha}_{ij}\widetilde{\alpha}_{ij} \rangle^3}. \tag{2.13}$$

Equations (2.10) and (2.13) complete the model with two-level test filters. In this approach, the model coefficient is globally constant in space but varies in time.

3. New dynamic model with a single test filter

In the proposed model, we start with the test-filtered incompressible Navier-Stokes and continuity equations:

$$\frac{\partial \widetilde{u}_i}{\partial t} = -\frac{\partial \widetilde{u}_i\widetilde{u}_j}{\partial x_j} - \frac{\partial \widetilde{p}}{\partial x_i} + \nu \frac{\partial^2 \widetilde{u}_i}{\partial x_j \partial x_j} - \frac{\partial T_{ij}}{\partial x_j}, \tag{3.1}$$

$$\frac{\partial \widetilde{u}_i}{\partial x_i} = 0, \tag{3.2}$$

where $\widetilde{()}$ denotes $\widehat{\overline{()}}$ and $T_{ij} = \widetilde{u_i u_j} - \widetilde{u}_i\widetilde{u}_j$.

The test-filter-level large-scale turbulent kinetic energy equation is

$$\frac{\partial \widetilde{u}_i\widetilde{u}_i}{\partial t} = \frac{\partial}{\partial x_j}\left\{ -\widetilde{u}_i\widetilde{u}_i\widetilde{u}_j - 2\widetilde{u}_j\widetilde{p} + \nu \frac{\partial \widetilde{u}_i\widetilde{u}_i}{\partial x_j} - 2T_{ij}\widetilde{u}_i \right\} - 2\nu \frac{\partial \widetilde{u}_i}{\partial x_j}\frac{\partial \widetilde{u}_i}{\partial x_j} + 2T_{ij}\widetilde{S}_{ij}. \tag{3.3}$$

Subtracting (3.3) from the test-filtered total kinetic energy equation results in a transport equation for T_{ii}:

$$\begin{aligned} \frac{\partial T_{ii}}{\partial t} = \frac{\partial}{\partial x_j}\left\{ -(\widetilde{u_i u_i u_j} - \widetilde{u}_i\widetilde{u}_i\widetilde{u}_j) - 2(\widetilde{u_j p} - \widetilde{u}_j\widetilde{p}) + \nu\left(\frac{\partial \widetilde{u_i u_i}}{\partial x_j} - \frac{\partial \widetilde{u}_i\widetilde{u}_i}{\partial x_j} \right) + 2T_{ij}\widetilde{u}_i \right\} \\ -2\nu\left(\widetilde{\frac{\partial u_i}{\partial x_j}\frac{\partial u_i}{\partial x_j}} - \frac{\partial \widetilde{u}_i}{\partial x_j}\frac{\partial \widetilde{u}_i}{\partial x_j} \right) - 2T_{ij}\widetilde{S}_{ij}. \end{aligned} \tag{3.4}$$

By subtrating test-filtered (2.8) from (3.4), one finally obtains a transport equation for L_{ii} $(= T_{ii} - \widehat{\tau}_{ii})$

$$\frac{\partial L_{ii}}{\partial t} =$$
$$\frac{\partial}{\partial x_j}\left\{-(\widehat{\overline{u}_i\overline{u}_i\overline{u}_j} - \widetilde{u}_i\widetilde{u}_i\widetilde{u}_j) - 2(\widehat{\overline{u}_j\overline{p}} - \widetilde{u}_j\widetilde{p}) + \nu\left(\frac{\partial\widehat{\overline{u}_i\overline{u}_i}}{\partial x_j} - \frac{\partial\widetilde{u}_i\widetilde{u}_i}{\partial x_j}\right) - 2(\widehat{\tau_{ij}\overline{u}_i} - T_{ij}\widetilde{u}_i)\right\}$$
$$-2\nu\left(\frac{\partial\widehat{\overline{u}_i}}{\partial x_j}\frac{\partial\widehat{\overline{u}_i}}{\partial x_j} - \frac{\partial\widetilde{u}_i}{\partial x_j}\frac{\partial\widetilde{u}_i}{\partial x_j}\right) + 2(\widehat{\tau_{ij}\overline{S}_{ij}} - T_{ij}\widetilde{S}_{ij}). \tag{3.5}$$

Taking the volume average of (3.5) assuming "global equilibrium" finally results in

$$C_v = -\frac{\nu}{2}\cdot\frac{\left\langle\widehat{\overline{\alpha}_{ij}\overline{\alpha}_{ij}} - \widetilde{\alpha}_{ij}\widetilde{\alpha}_{ij}\right\rangle}{\left\langle\widehat{\overline{\Pi}\overline{S}_{ij}\overline{S}_{ij}} - \widetilde{\Pi}\widetilde{S}_{ij}\widetilde{S}_{ij}\right\rangle}, \tag{3.6}$$

where the subgrid-scale quantities $\overline{()}$ are defined in (2.7) and

$$T_{ij} - \frac{1}{3}T_{kk}\delta_{ij} = -2C_v\widetilde{\Pi}\widetilde{S}_{ij},$$
$$\widetilde{\Pi} = \sqrt{\frac{\widetilde{B}_\beta}{\widetilde{\alpha}_{kl}\widetilde{\alpha}_{kl}}},$$
$$\widetilde{B}_\beta = \widetilde{\beta}_{11}\widetilde{\beta}_{22} - \widetilde{\beta}_{12}\widetilde{\beta}_{12} + \widetilde{\beta}_{11}\widetilde{\beta}_{33} - \widetilde{\beta}_{13}\widetilde{\beta}_{13} + \widetilde{\beta}_{22}\widetilde{\beta}_{33} - \widetilde{\beta}_{23}\widetilde{\beta}_{23},$$
$$\widetilde{\beta}_{ij} = \sum_{m=1}^{3}\widetilde{\Delta}_m^2\widetilde{\alpha}_{mi}\widetilde{\alpha}_{mj},$$
$$\widetilde{\alpha}_{ij} = \frac{\partial\widetilde{u}_j}{\partial x_i}. \tag{3.7}$$

The present model coefficient is dynamically determined from the instantaneous flow field and computational resolution by utilizing only a single-level test filter.

Figure 1 shows the temporal evolution of the model coefficient predicted by (3.6) for turbulent channel flow at $Re_\tau = 395$ after the flow has reached a statistically steady state. The temporal variation of the model coefficient is mild and the mean value of the coefficient is approximately 0.05, which differs from the value of 0.07 proposed by Vreman (2004) for channel flow and mixing layer simulations. The present dynamic model shows favorable agreement with the direct numerical simulation results of Moser *et al.* (1999) (see section 4.1 for details).

The present model shares the important features of the original Vreman model (Vreman 2004) and the dynamic model of Park *et al.* (2006). Even with the spatially constant model coefficient, the model predicts zero eddy viscosity in regions where the vanishing eddy viscosity is theoretically expected. For example, figure 2*a* shows the instantaneous spanwise vorticity contours of the flow over a circular cylinder. The flow configuration consists of a variety of different flow regimes such as laminar uniform flow (Ω_l), laminar boundary layer ($\partial\Omega_w$), and turbulent wake (Ω_t). The present model predicts vanishing

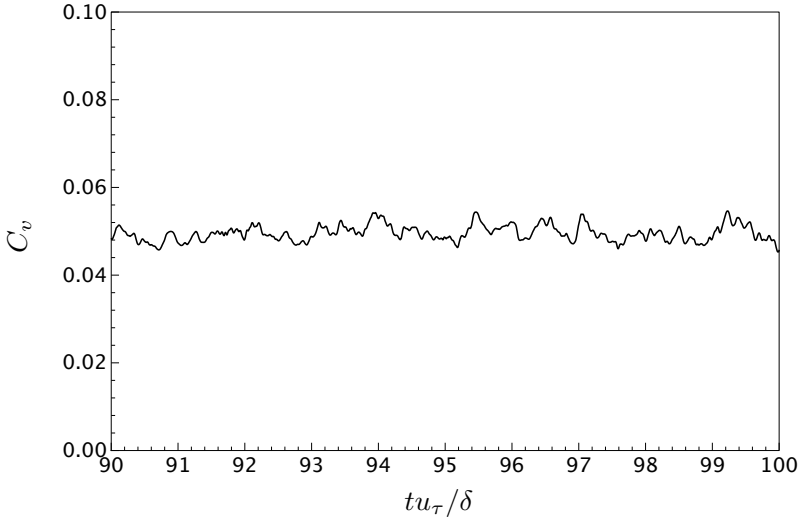

FIGURE 1. Temporal evolution of C_v predicted by the present dynamic procedure for turbulent channel flow at $Re_\tau = 395$.

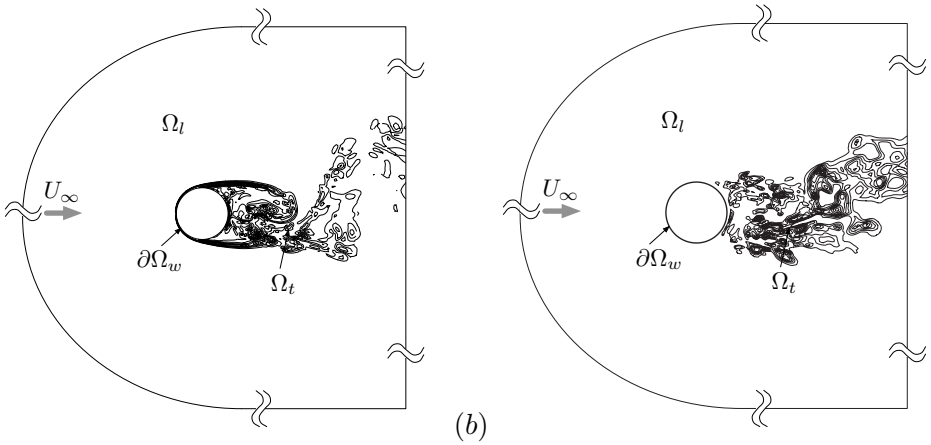

FIGURE 2. Contour plots of (a) the instantaneous spanwise vorticity and (b) the ratio of eddy viscosity to molecular viscosity ν_T/ν predicted by large-eddy simulation with the present dynamic model in the circular cylinder flow at $Re_D = 3900$. 20 contour levels in the range of $-20 \sim 20$, and $0.5 \sim 5$ are shown in (a) and (b), respectively. Ω_l, Ω_t, and $\partial\Omega_w$ represent laminar uniform, turbulent wake, and boundary layer flow regimes, respectively.

eddy viscosity in the regions of laminar flow (Ω_l and $\partial\Omega_w$) as shown in figure 2b. The large-eddy simulation of circular cylinder flow is discussed in detail in section 4.2.

Besides the advantage of utilizing only a single-level test filter, which improves the applicability of the model for complex flow configurations (especially with unstructured grid topology where defining the second-level test filter is not straightforward), the present volume-averaging process in (3.6) obviates a possibility of obtaining different model coefficients when two different computational domains that contain the same turbulence flow field but different laminar shear flow regions are employed. This is because both the viscous dissipation ($\nu(\widehat{\overline{\alpha}_{ij}\overline{\alpha}_{ij}} - \widetilde{\alpha}_{ij}\widetilde{\alpha}_{ij})$) and the subgrid-scale dissipation ($\widehat{\overline{\Pi}\widetilde{S}_{ij}\widetilde{S}_{ij}} - \widetilde{\Pi}\widetilde{S}_{ij}\widetilde{S}_{ij}$)

Re_τ	L_x	L_y	L_z	N_x	N_y	N_z	Δx^+	Δy^+_{min}	Δz^+
590	$2\pi\delta$	2δ	$\pi\delta$	64	97	64	57	0.59	29
395	$2\pi\delta$	2δ	$\frac{2}{3}\pi\delta$	48	65	48	48	0.95	18

TABLE 1. Grid parameters for large-eddy simulation of turbulent channel flows. L_x, L_y, and L_z are the streamwise, vertical, and spanwise domain sizes, respectively. $N_{x(y,z)}$ and $\Delta x(y,z)^+$ are the number of mesh points and the resolution in wall units, respectively.

in (3.6) vanish in the laminar flow region. Therefore, in the present method, the regions where both the subgrid-scale dissipation and the viscous dissipation vanish are naturally excluded from the averaging process in (3.6). In the dynamic model of Park *et al.* (2006), the influence of the computational domain size in the volume-averaging procedure is controlled by γ in (2.10).

4. Results and discussion

4.1. *Large-eddy simulation of turbulent channel flow*

Turbulent flow through a plane channel has been widely considered as a benchmark for validating turbulence models. Reynolds numbers of 590 and 395 based on the channel half height δ and friction velocity u_τ are considered. Large-eddy simulation results with three different Vreman-type closures including the present dynamic model and the dynamic Smagorinsky model (Germano *et al.* 1991) with Lilly (1992)'s modification are compared with the direct numerical simulation results of Moser *et al.* (1999). The computational parameters for large-eddy simulations at the two different Reynolds numbers are summarized in table 1. For the simulation at $Re_\tau = 590$, a second-order finite-volume solver (Mahesh *et al.* 2006) on a collocated grid arrangement of the primary variables is employed, while a second-order finite-difference solver (Templeton *et al.* 2006) on a staggered grid is used in the case of $Re_\tau = 395$.

In figure 3, the profiles of the mean streamwise velocity and rms velocity fluctuations at $Re_\tau = 590$ obtained using the present dynamic model, the dynamic model of Park *et al.*, the Vreman model with a fixed coefficient of 0.07, and the dynamic Smagorinsky model are compared with the direct numerical simulation data of Moser *et al.* (1999). The time-averaged model coefficients for the present channel flow are much smaller than the coefficient suggested by Vreman (2004) (0.07), and are 0.010 and 0.008 in the present dynamic model and Park *et al.*'s dynamic model, respectively. The present dynamic model (solid line) and the dynamic model of Park *et al.* (dashed line) predict similar results. The collocated grid method used in the present simulation requires finer resolution in the spanwise direction to predict similar results predicted by the staggered grid approach (Ham & Iaccarino 2004). The present and Park *et al.*'s dynamic models predict superior results to those obtained with the Vreman model (chain-dotted line) with the coefficient of 0.07, which is not optimal in the present simulation. The present results are comparable or superior to those obtained with the dynamic Smagorinsky model (dotted line). In the mean velocity profile, the upward shift in the log-layer is a little bit smaller than that of the dynamic Smagorinsky model, while the Vreman model with a non-optimal model

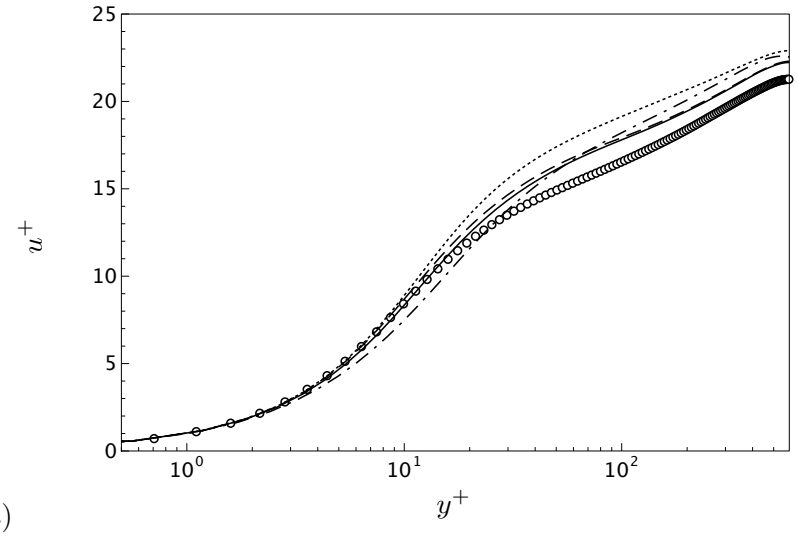

(a)

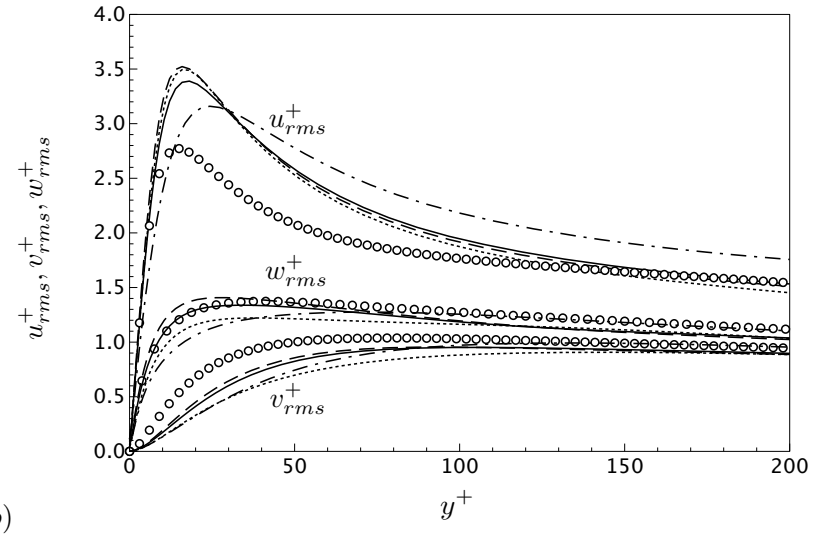

(b)

FIGURE 3. Profiles of (*a*) the mean streamwise velocity and (*b*) rms velocity fluctuations in turbulent channel flow at $Re_\tau = 590$. Solid line, the present dynamic model; dashed line, dynamic model of Park *et al.*; dotted line, dynamic Smagorinsky model; chain-dotted line, Vreman model with $C_v = 0.07$; symbol, direct numerical simulation (Moser *et al.* 1999).

coefficient ($C_v = 0.07$) predicts deficiency both in the mean streamwise velocity and rms velocity fluctuations, which are under-predicted in the overlap layer.

The time-averaged model coefficients for the channel flow at $Re_\tau = 395$ are approximately 0.05 in both the present dynamic model and the dynamic model of Park *et al.* Also at this Reynolds number, the present dynamic and Park *et al.*'s dynamic models are slightly superior to the dynamic Smagorinsky model in predicting the mean and turbulence statistics provided by the direct numerical simulation of Moser *et al.* (1999).

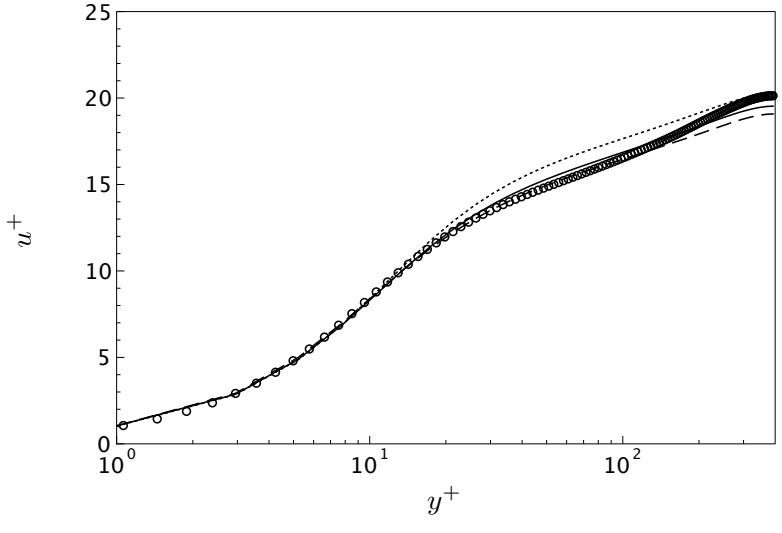

(*a*)

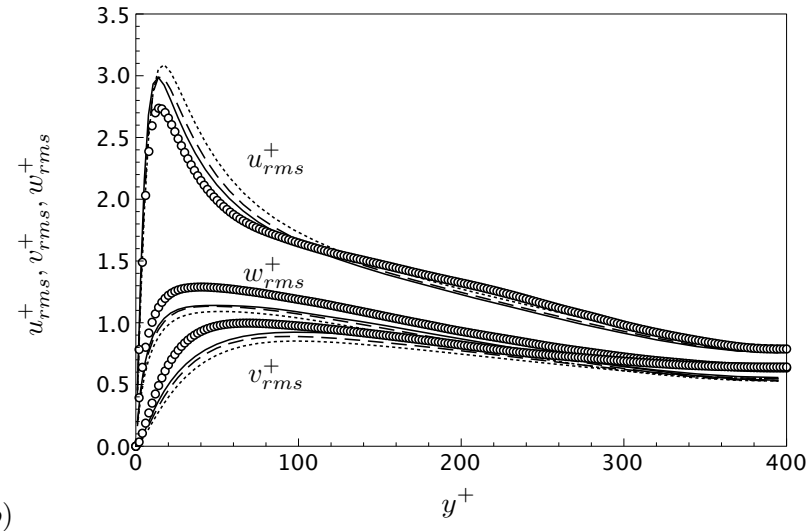

(*b*)

FIGURE 4. Profiles of (*a*) the mean streamwise velocity and (*b*) rms velocity fluctuations in turbulent channel flow at $Re_\tau = 395$. Solid line, the present dynamic model; dashed line, dynamic model of Park *et al.*; dotted line, dynamic Smagorinsky model; symbol, direct numerical simulation (Moser *et al.* 1999).

4.2. *Large-eddy simulation of flow over a circular cylinder*

The effectiveness of the present dynamic model is further assessed in the large-eddy simulation of flow over a circular cylinder at $Re_D = 3900$. The circular cylinder flow consists of a variety of flow regimes including laminar unifrom flow, laminar boundary layer, laminar shear layer, transition, and turbulent wake. Therefore, it is an excellent benchmark for assessing the predictive capability of the proposed subgrid-scale model. Results predicted by the present dynamic model are compared with those predicted by the large-eddy simulation performed with the dynamic Smagorinsky model and a high-order

L_x	L_y	L_z	N_θ	N_z	$N_{BL}(\theta = 90^\circ)$	$N_{BL}(\theta = 170^\circ)$	N_{total}
$-30D \sim 20D$	$-30D \sim 30D$	πD	300	65	24	13	7,543,680

TABLE 2. Grid parameters for cylinder flow simulation at $Re_D = 3900$. L_x, L_y, and L_z are the streamwise, vertical, and spanwise domain sizes, respectively. N_θ, N_z, and N_{BL} are the numbers of mesh points in the circumferential and spanwise directions and in the boundary layer, respectively. N_{total} denotes the total number of mesh points.

	$\overline{C}_D$	$C_{L_{rms}}$	$-C_{pb}$	St
LES with DM1	1.01	0.12	0.92	0.211
LES with DSM*	1.04	·	0.94	0.210
Experiments	$0.99 \pm 0.05^\dagger$	$0.1 \pm 0.05^\dagger$	$0.88 \pm 0.05^\dagger$	$0.215 \pm 0.05^\ddagger$

TABLE 3. Summary of cylinder flow computations at $Re_D = 3900$. $\overline{C_D}$, $C_{L_{rms}}$, $-C_{pb}$, and St are the mean-drag, rms-lift, base-pressure coefficients and the Strouhal number, respectively. DM1 and DSM denote the present dynamic model and the dynamic Smagorinsky model, respectively. *Kravchenko & Moin (2000), †Norberg (1987), and ‡Ong & Wallace (1996).

numerical scheme (B-spline method; Kravchenko & Moin 2000) and experimental data (Norberg 1987; Ong & Wallace 1996). Grid parameters used in the present simulation are summarized in table 2. The numerical method is a second-order finite-volume method and an unstructured grid is employed (Ham & Iaccarino 2004). The total number of grid points is similar to those employed in other previous large-eddy simulations performed with a second-order finite-difference method (Kim & Choi 2005; Park *et al.* 2006).

As shown in figure 2, the present model predicts eddy-viscosity distribution that is qualitatively expected from the physical characteristics of the flow (figure 2). High levels of eddy viscosity occur in the turbulent near wake. On the other hand, Beaudan & Moin (1994) found, with a constant-coefficient Smagorinsky model, that the largest mean eddy viscosity is generated in the separated shear layers that are laminar at $Re_D = 3900$. In the simulation with the present dynamic model, the peak ratio of the eddy viscosity to the molecular viscosity is not greater than 5 (figure 2).

The global flow quantities such as the drag, rms-lift, base pressure coefficients, and the Strouhal number are compared with numerical (Kravchenko & Moin 2000) and experimental data (Norberg 1987; Ong & Wallace 1996) and are summarized in table 3. In general, the present simulation results are in favorable agreement with the other numerical and experimental data.

The profiles of the mean streamwise velocity and streamwise velocity fluctuations obtained in three different near-wake locations are compared with the numerical data of Kravchenko & Moin (2000) in figure 5. The present large-eddy simulation with the dynamic model performs well and predicted comparable results to those predicted by Kravchenko & Moin (2000) with the dynamic Smagorinsky model. However, it is worth

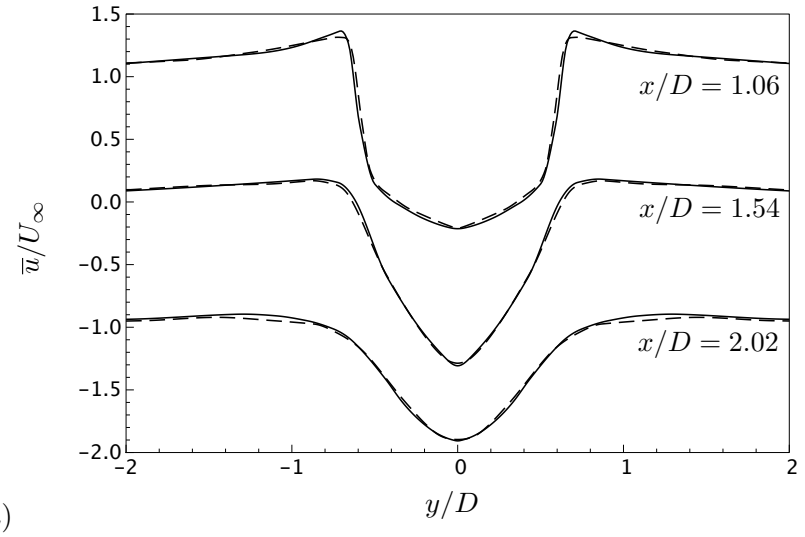

(*a*)

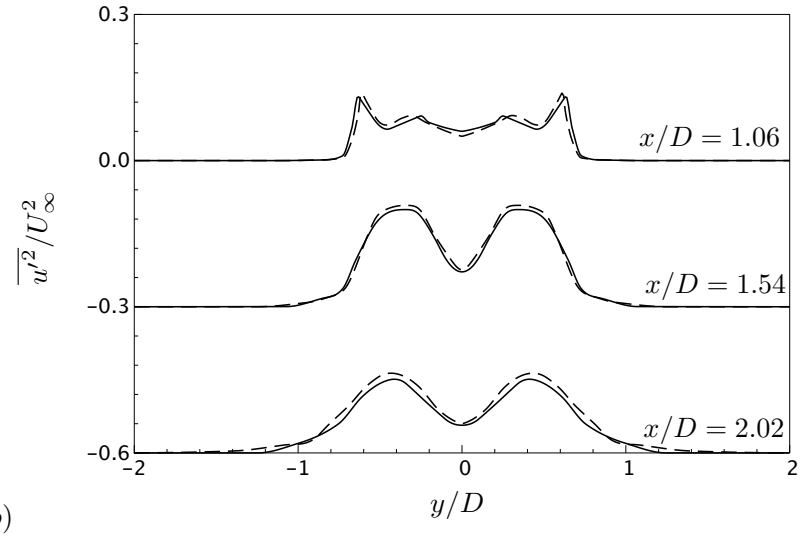

(*b*)

FIGURE 5. Profiles of (*a*) the mean streamwise velocity and (*b*) streamwise-velocity fluctuations at three locations in the wake of a circular cylinder at $Re_D = 3900$. Solid line, large-eddy simulation with the present dynamic model; dashed line, large-eddy simulation with the dynamic Smagorinsky model (Kravchenko & Moin 2000).

noting that, in the large-eddy simulation of Kravchenko & Moin (2000), it was necessary to discard negative model coefficients by ad hoc clipping operations for numerical stability (Kravchenko & Moin 1998).

5. Summary

A dynamic procedure for closure of the subgrid-scale model developed by Vreman (2004) using a single-level test filter has been proposed. The dynamic procedure of determining model coefficient is based on the "global equilibrium" between the subgrid-scale

dissipation and the viscous dissipation as utilized by Park *et al.* (2006). Like the fixed-coefficient (Vreman 2004) and dynamic-coefficient (Park *et al.* 2006) Vreman models, the present model predicts zero eddy-viscosity in regions where the vanishing eddy viscosity is theoretically expected. In contrast to the dynamic procedure by Park *et al.* (2006), which employs two-level test filters, the present model necessitates only a single-level test filter, and therefore is more suitable for large-eddy simulation in complex geometries. The present model is not more complicated than the dynamic Smagorinsky model in implementation and does not require any ad hoc spatial and temporal averaging or clipping of the model coefficient for numerical stabilization. In addition, the computational cost is not more expensive than that of the dynamic Smagorinsky model. The present dynamic procedure has been found quite effective in determining the model coefficient and predicted excellent results in large-eddy simulations of turbulent channel flow and flow over a circular cylinder.

Acknowledgments

The authors would like to thank Professor Haecheon Choi for allowing us to access the preprint of Park *et al.* [Phys. Fluids **18**, 125109 (2006)].

REFERENCES

Beaudan, P. & Moin, P. 1994 Numerical experiments on the flow past a circular cylinder at sub-critical Reynolds number. Report TF-62. Department of Mechanical Engineering, Stanford University, Stanford, California.

da Silva, C. B. & Metais, O. 2002 On the influence of coherent structures upon interscale interaction in turbulent plane jets. *Journal of Fluid Mechanics* **473**, 103–145.

Germano, M., Piomelli, U., Moin, P. & Cabot, W. H. 1991 A dynamic subgrid-scale eddy-viscosity model. *Physics of Fluids A* **3** (7), 1760–1765.

Ghosal, S., Lund, T. S., Moin, P. & Akselvoll, K. 1994 A dynamic localization model for large-eddy simulation of turbulent flows. *Journal of Fluid Mechanics* **282**, 1–27.

Ham, F. & Iaccarino, G. 2004 Energy conservation in collocated discretization schemes on unstructured meshes. Annual Research Briefs, 3–14, Center for Turbulence Research, Stanford, California.

Kim, J. & Choi, H. 2005 Distributed forcing of flow over a circular cylinder. *Physics of Fluids* **17**, 033103.

Kravchenko, A. G. & Moin, P. 1998 B-spline methods and zonal grids for numerical simulations of turbulent flows. Report TF-73. Department of Mechanical Engineering, Stanford University, Stanford, California.

Kravchenko, A. G. & Moin, P. 2000 Numerical studies of flow over a circular cylinder at $Re_D = 3900$. *Physics of Fluids* **12** (2), 403–417.

Lilly, D. K. 1992 A proposed modification of the Germano subgrid-scale closure model. *Physics of Fluids A*, **4** (3), 633–635.

Mahesh, K., Constantinescu, G., Apte, S., Iaccarino, G., Ham, F. & Moin, P. 2006 Large-eddy simulation of reacting turbulent flows in complex geometries. *Journal of Applied Mechanics* **73**, 374–381.

Meneveau, C., Lund, T. S. & Cabot, W. H. 1996 A Lagrangian dynamic subgrid-scale model of turbulence. *Journal of Fluid Mechanics* **319**, 233–242.

Moin, P. 2002 Advances in large eddy simulation methodology for complex flows. *International Journal of Heat and Fluid Flow* **23**, 710–720.

Moser, R. D., Kim, J. & Mansour, N. N. 1999 Direct numerical simulation of turbulent channel flow up to Re_τ=590. *Physics of Fluids* **11** (4), 943–945.

Norberg, C. 1987 Effects of Reynolds number and a low-intensity freestream turbulence on the flow around a circular cylinder. Publication 87/2. Department of Applied Thermodynamics and Fluid Mechanics, Chalmers University of Technology, Sweden.

Ong, L. & Wallace, J. 1996 The velocity field of the turbulent very near wake of a circular cylinder. *Experiments in Fluids* **20**, 441–453.

Park, N., Lee, S., Lee, J. & Choi, H. 2006 A dynamic subgrid-scale eddy-viscosity model with a global model coefficient. *Physics of Fluids* **18**, 125109.

Piomelli, U., Yu, Y. & Adrian, R. J. 1996 Subgrid-scale energy transfer and near-wall turbulence structure. *Physics of Fluids* **8**(1), 215–224.

Templeton, J. A., Wang, M. & Moin, P. 2006 An efficient wall model for large-eddy simulation based on optimal control theory. *Physics of Fluids* **18**, 025101.

Vreman, A. W. 2004 An eddy-viscosity subgrid-scale model for turbulent shear flow: algebraic theory and applications. *Physics of Fluids* **16** (10), 3670–3681.

You, D., Mittal, R., Wang, M. & Moin, P. 2004 Computational methodology for large-eddy simulation of tip-clearance flows. *AIAA Journal* **42** (2), 271–279.